Additive Manufacturing 77 (2023) 103803

Contents lists available at ScienceDirect

Additive Manufacturing

journal homepage: www.elsevier.com/locate/addma

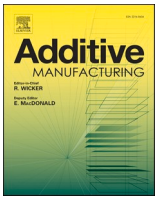

Expanding the pharmaceutical formulation space in material extrusion 3D printing applications

Elke Prasad [a,b,*], John Robertson [a,b], Alastair J. Florence [a,b], Gavin W. Halbert [a,b]

[a] EPSRC Future Manufacturing Research Hub, University of Strathclyde, Technology and Innovation Centre, 99 George Street, Glasgow G1 1RD, UK
[b] Strathclyde Institute for Pharmacy and Biomedical Sciences, University of Strathclyde, 161 Cathedral Street, Glasgow G4 0RE, UK

ARTICLE INFO

Keywords:
Melt extrusion
Filament free 3D printing
Affinisol™ 15LV
Oral solid dose form
Rheology

ABSTRACT

The two major drawbacks of filament based material extrusion printing in pharmaceutical manufacturing are a) the additional manufacturing step of the filament prior to printing and b) the limited pharmaceutical formulation space due to unsuitable (mechanical and rheological) properties. Although formulation strategies can address some of these issues, they require heavily formulated or complex systems, which require time and resource to solve/overcome. In this study we present a novel, filament free 3D printing system, obviating limitations of unsuitable filament properties and opening up the pharmaceutical formulation space in material extrusion of pharmaceutical oral solid dose forms (OSDs). Prasad et al. reported on a 30% w/w Paracetamol (PCM) in Affinisol™ HPMC HME 15LV (30PCM-AFF) formulation, not printable on a conventional filament based material extrusion printer. This formulation was processed on the filament free 3D printer to successfully print OSDs. In initial rheological screening tests, process conditions for initial printing trials were identified. The operating space of the filament free 3D printer and slicer settings in this process were investigated as well as the uniformity of mass and dimensions of printed OSDs. A relationship of Slicer Infill percentage (microstructure) and tablet core weight was also assessed, demonstrating the ability to create patient centred dose forms. Material reconciliation showed good traceability of material during the manufacturing process.

1. Introduction

Additive manufacturing (3D printing) has, in recent years, gained interest in the scientific community [1–4]. In the pharmaceutical field, this technique enables not only personalisation of medicines in terms of adjusting the dose of active pharmaceutical ingredient (API), but also affords the possibility to fine tune product performance through advanced micro-structure control of the tablet core [3,5,6]. The technology also offers a platform for early phase clinical trial dose escalation studies employing a single formulation in a single manufacturing step.

The most common type of additive manufacturing technique is ‘filament fused fabrication’ (FFF) due to its lower cost, accessibility and higher reproducibility [4]. FFF printers are commercially readily available at relatively low cost. These printers operate with polymer feedstock material in the shape of a filament (Fig. 1). Commercially available filaments with ideal material properties for 3D printing, such as Polylactic Acid (PLA) and Acrylonitrile butadiene styrene (ABS), are not suitable for pharmaceutical applications.

For pharmaceutical applications, the feedstock material can be produced via a Hot-Melt-Extrusion (HME) manufacturing step prior to 3D printing oral solid dose (OSD) forms [4]. This HME process allows to manufacture filaments with drug loadings of up to 50% w/w in pharmaceutically approved polymers [7–11].

During an FFF process, the filament feedstock material is fed into the hot end of the printer via a spring-loaded pinch-wheel drive gear (Fig. 1). As the drive gear wheels turn, the filament is moved forward into the hot end, where the material is softened or molten. The upper, solid part of the filament acts as a piston to push the softened/melted material out of the nozzle onto a print bed or substrate laying down layer upon layer of material to create a 3D object. In order for this process to work, these filaments require very specific properties in size and shape, but also suitable mechanical and rheological properties to successfully convey the filament into the hot end and deposit material on the print bed.

This process fails when the mechanical properties of the filaments are not favourable, such as brittle fracture or ductile failure (Fig. 1) in

* Corresponding author at: EPSRC Future Manufacturing Research Hub, University of Strathclyde, Technology and Innovation Centre, 99 George Street, Glasgow G1 1RD, UK.
E-mail address: elke.prasad@strath.ac.uk (E. Prasad).

https://doi.org/10.1016/j.addma.2023.103803
Received 7 June 2023; Received in revised form 1 September 2023; Accepted 30 September 2023
Available online 2 October 2023

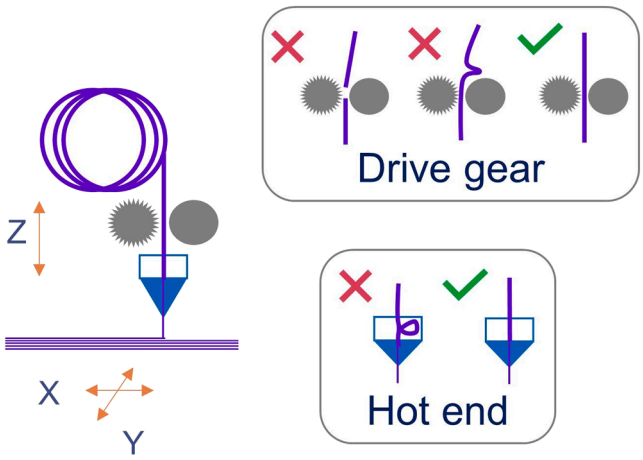

Fig. 1. Schematic of Fused Filament Fabrication (FFF) process and filament failure in the drive gear and hot end.

the drive gear [1,7,12–20]. The FFF process also fails when the relationship of mechanical properties to the melt viscosity is unfavourable and the material buckles in the hot end of the printer [7].

The pharmaceutical formulation space for FFF 3D printing system is often limited due to these unsuitable filament properties of simple (binary) formulations. In recent years, a number of studies aimed to define specific mechanical filament properties for successful FFF application [21], such as a minimum strain at a yield of 5% [22,23], a high Young's Modulus [24,25], or Flexural modulus [7]. However, this resulted in limited success since a multitude of other factors impact the FFF process, such as: the relationship of mechanical to rheological properties [26], the heat transfer (of Non-Newtonian fluids) in the hot end [27], the relationship of drag and pressure flow patterns with the ability to cause backflow in the hot end [28], differences in shear between hot end wall and the core of the filament, as well as the non-isothermal nature of the process [27]. Overcoming these limitations requires time and resource, as not only the formulation is refined, but also a filament manufacturing process is developed.

The formulation space for FFF suitable filaments for pharmaceutical applications, particularly for immediate release formulations, is limited, since many immediate release polymers, such as Polyvinyl alcohol (PVA), Co-povidone (Plasdone S-630 Ultra, Kollidon-VA64) or polyvinyl caprolactam-polyvinyl acetate-polyethylene glycol graft co-polymer (Soluplus®), exhibit brittle mechanical properties [12,29,30]. Brittle behaviour has also been described for Kollidon-VA64 and Eudragit EPO [12,13]. Formulation approaches can overcome unsuitable mechanical properties. In the case of brittle failure of feedstock filaments, incorporating plasticisers (mannitol, sorbitol, triethylcitrate (TEC), acetyltriethylactylcitrate (ATEC), triacetin, polyethylene glycol (PEG), poly ethylene oxide (PEO), polysorbate 80 (Tween 80), glycerol, stearic acid) into the polymer matrix can alter mechanical properties [3,31–34].

Limitations in the formulation space can also occur for cases where specific drug loading ranges result in heavily plasticised and very soft (ductile) filaments. Prasad et al. reported on the printability of filaments containing 10 – 50% (w/w) Paracetamol (PCM) in Affinisol™ HPMC HME 15LV (Affinisol™, a Hydroxypropyl Methylcellulose (HPMC) polymer) in a conventional FFF printer. Filaments with medium drug loading from 25% to 40% (w/w) failed to print due to high ductility and low mechanical strength [7]. These ductile filaments buckled in the hot end of the FFF printer (Fig. 1). Similar ductile failures have been reported in the literature [12,35], where filaments with low stiffness were challenging to print and their printability or possible process conditions strongly depended on their viscosity [36]. In these instances, the relationship of mechanical to rheological properties of the formulation, described by Venkataraman et al. as the buckling ratio [37], were unfavourable.

These issues are often addressed by developing complex formulations, by adding fillers, such as Lactose, Talc, tricalcium phosphate (TCP) and microcrystalline cellulose (MCC) [38–41] or working with polymer blends [13,42,43] to achieve suitable mechanical properties by increasing stiffness and strength and improving rheological properties [39–41,44–46]. Additional excipients, like lubricants or super disintegrants may also be added depending on the need of the formulation [3,47].

In these instances, excipients are added solely to afford suitable mechanical and rheological properties of the filament feedstock material, potentially reducing drug loading and release profiles of final dose forms [35]. Complex formulations are not desirable as multiple excipients require purchasing, testing and certifying prior to pharmaceutical manufacture demanding additional time and resource. It is not only the formulation development that adds to the increase in resources in many instances, but also the filament manufacturing step and the associated quality checks and stability testing of an intermediate product prior to the 3D printing step. Mechanical properties may change over time due to high water sorption capacity of polymers or APIs, with the absorbed water acting as a secondary plasticiser, rendering the filament unsuitable for FFF application and may also facilitate microbial growth and potentially altering drug stability [21,25,48,49]. Solid state drug stability with changes from amorphous to crystalline have shown to not only affect the mechanical properties but also the release properties of the filament [21]. Additionally, filament surface properties, diameter and sphericity of filament can also have an impact on the printing process and quality of the resulting product [50,51].

Recent developments in this area aimed to develop filament free melt extrusion printers to overcome these issues. FabRx developed the M3DIMAKER™, a small scale batch printer based on the principle of a single screw powder extruder, processing powder blends into 3D printed dose forms in a single step [52,53]. A study using a similar single screw extruder was published by Pistone et al. [54]. Fanous et al. used powder filled cartridges in combination with a pneumatic piston dosing system to successfully produce 3D printed dose forms by melt extrusion [35]. Triastek developed a Melt Extrusion Deposition (MED™) system and produced different dose form microstructures in combination with different formulation compositions to target specific drug release profiles [55].

In this study we present a novel, filament free 3D printing system (Intellectual Property Office UK, patent application number 2101534.2), overcoming limitations of unsuitable filament properties, specifically ductile filament failure. This eliminates the requirement for specific mechanical properties of filament feedstock, therefore opening up the pharmaceutical formulation space in FFF to a wider range of simple (binary) formulations. A "non-printable" formulation (30PCM-AFF [7]) was processed on the filament free 3D printer to successfully print Oral Solid Dose forms (OSD). In initial rheological screening tests, process conditions for initial printing trials were identified. The operating space of the filament free 3D printer and slicer settings in this process were investigated as well as the uniformity of mass and dimensions of printed OSDs. A relationship of Slicer Infill percentage (microstructure) and tablet core weight was also assessed, demonstrating the ability to create patient centred dose forms. Material reconciliation showed minimal material requirements during start-up of the manufacturing process.

2. Materials and methods

2.1. Materials

Acetaminophen (Paracetamol, PCM) was purchased from Mallinckrodt Inc., USA: PCM powder grade, Polymorph Form I, Particle size D (0.5) of 52.6 μm. Hydroxypropyl methylcellulose (HPMC), grade Affinisol™ 15LV, a water soluble, amorphous polymer with a molecular weight of.

less than 100 kDa, bulk density of 0.42 kg/l and D(0,5) of 104.49 μm, was kindly donated by Dow Chemical Company ("Dow"). All chemicals were used as received.

2.2. Formulation composition and blending

Powders were passed through a 1 mm mesh sieve prior to weighing. 30% (w/w) PCM in Affinisol™ 15LV (PM 30PCM-AFF) was prepared by mixing in a Pharmatech bin blender AB-015 equipped with a 5 L vessel for 150–200 g samples. Blending was carried out at 25 rpm with an agitator speed of 100 rpm for 20 min. Extrudate samples of 30% (w/w) PCM in Affinisol™ 15LV (EX 30PCM-AFF) had previously been prepared by Prasad et al. [7].

2.3. Rheology

Physical mixtures (PM 30PCM-AFF) and extrudates (EX 30PCM-AFF) [7] were analysed on a Haake Mars III rotational rheometer equipped with a 25 mm diameter parallel plate geometry. 500 mg of powdered sample were compacted under vacuum (400 mbar) with a compaction force of 3.9227 kN for 1 min using a manual hydraulic press to prepare round, 25 mm diameter discs for analysis. In the case of extrudate samples, 500 mg of pelletised extrudates were manually added to the plate geometry. Zero gap height calibrations were performed prior to rheological analysis. Measurements were performed in the linear visco-elastic region (LVR) of materials.

2.3.1. Oscillatory temperature sweep

Oscillatory temperature sweep: Sample discs were loaded at 190 °C and equilibrated at temperature prior to analysis. Temperature sweeps were performed from 190 °C to 95 °C temperature, with a constant deformation of 0.5% at a frequency of 1 Hz and a cooling rate of 5 °C/min. The gap setting was normal force controlled at 0.1 N.

2.3.2. Oscillatory frequency sweep

Oscillatory frequency sweeps: Sample discs were loaded at test temperature and equilibrated at temperature prior to analysis. Frequency sweeps were performed with a constant deformation of 0.5% across a frequency range from 0.1 to 100 Hz. Frequency sweeps were performed at 140 °C, 150 °C, 160 °C, 170 °C, 180 °C, 190 °C.

2.4. Bulk density

Bulk density was measured by carefully adding approximately 100 mL of powder to a 250 mL glass measuring cylinder. The exact volume and weight of the powder was determined, and the bulk density calculated as ρ bulk = weight (g) / volume (mL) = [g/mL = kg/L].

2.5. Slicer software

'CURA for Startt' slicer software (1.1.1) was used to convert STL files (3D-object) into a suitable gcode file format for the filament free 3D printer software. Manual modification of the gcode file was performed to enable communication with the Duet 2 (Duet3D Ltd, UK) controller interface.

2.6. HME – 3DP

Hot melt extrusion was performed on a Process 11 (Thermo Fisher, Karlsruhe, Germany) twin screw extruder with a length (L) to diameter (D) ratio of 40 ¾ equipped with a custom made (3D-printer) die. The screw configuration [29] consisted of: 14 feed screws - 6 × 60° F mixing elements - 7 x feed screws – 3 × 30° F, 3 × 60 ° F, 4 × 90 ° mixing elements – 13 feed screws - discharge element. A 2000 Series melt pressure transducer with a pressure limit of 100 bar (Terwin Instruments Ltd, Bottesford, UK) was attached to the HME die zone. The custom-made die contained a metering device which facilitated material deposition onto a print bed. The metering device and print bed were controlled through a Duet 2 controller (Duet3D Ltd, UK) (Intellectual Property Office UK, patent application number 2101534.2).

Physical mixture of the formulation was fed into the HME process using a Brabender Loss in weight (LIW) feeder machine (type DDW-N-MT) equipped with twin concave screws (TC12/12) (Brabender, Duisburg, Germany) and calibrated for maximum output prior to processing. HME process torque data was expressed as % of maximum torque (12 Nm). The 3D printer bed was equipped with a Tresbro Creality 3D Printer Flexible Magnetic Hot Bed (Shenzhen, China).

2.6.1. Initial printing trials

The print head of the filament free 3D printer was equipped with a 0.4 mm diameter, round nozzle. The process temperature for initial printing trials was based on the rheological properties of 30PCM-AFF physical mixture and extrudate. A simple 3D object, a cylinder (diameter 13 mm, height 4 mm, Fig. 7A), was chosen to identify suitable process parameters and slicer settings (Table 1). A slicer Infill percentage of 50% was used to print tablets and the uniformity of mass and dimensions was assessed.

Uniformity of dimensions was assessed by measuring the tablet dimensions using digital callipers (0.01 mm, Axminster, Devon, UK). Uniformity of mass was assessed by individually weighing 10 dosage forms on a 2DP analytical balance. The average mass (avg), standard deviation (stdev) and relative standard deviation (% RSD) were calculated. The minimum and maximum % deviation from the average tablet mass was also reported.

2.6.2. Printing at 145 °C, complex tablet shape

In an effort to prevent discolouration of the printed structures, subsequent printing studies were performed at 145 °C. In addition, a more complex, pharmaceutically relevant, tablet shape, an elliptical shape with rounded edges (Fig. 7B), was used.

2.6.3. Operating space – slicer settings at 145 °C

The operating space for slicer settings were investigated covering a layer height range of 0.2–0.6 mm and a print speed of 20 mm/s and 40 mm/s (Table 2).

2.6.4. Infill percentage versus tablet weight

The relationship of slicer Infill percentage to tablet core weight was investigated, ranging from 20% to 70% Infill percentage. Tablets with varying Infill percentage were printed in triplicate. The weight of each tablet was recorded on a 2DP analytical balance and the average determined.

2.6.5. Optical imaging of tablets

Optical images were obtained using a Leica M165 optical microscope equipped with Leica MC170HD camera set. Images were analysed using LAS v.4.8 software (Leica).

Table 1
Printing settings for initial printing trials of tablet structure A at 165 °C.

Print temperature 165 °C	Tablet structure A Layer height	
Print speed	**0.2 mm**	**0.4 mm**
20 mm/s	Tablet A, 50% Infill	Tablet A, 50% Infill
40 mm/s	Tablet A, 50% Infill	Tablet A, 50% Infill

Table 2
Printing settings for tablet structure B at 145 °C.

Print temperature 145 °C	Tablet structure B, Layer height				
Print speed	**0.2 mm**	**0.3 mm**	**0.4 mm**	**0.5 mm**	**0.6 mm**
20 mm/s	Tablet B, 50% Infill	Tablet B, 50% Infill	Tablet B, 20 – 70% Infill	Tablet B, 50% Infill	Tablet B, 50% Infill
40 mm/s	Tablet B, 50% Infill	Tablet B, 50% Infill	Tablet B, 50% Infill	Tablet B, 50% Infill	Tablet B, 50% Infill

3. Results

3.1. Rheology

3.1.1. Oscillatory temperature sweep

The complex viscosity of neat Affinisol™ 15LV polymer across the investigated temperature range, increased from ~$2.0 \cdot 10^3$ Pa·s at 190 °C to ~$7.5 \cdot 10^5$ Pa·s at 105 °C (Fig. 2). Between 105 and 95 °C, a plateau in complex viscosity was reached (Fig. 2), exemplifying a solidification of the formulation. This plateau was not observed when 30% w/w PCM was added to Affinisol™ 15LV. Instead, a downward shift of the complex viscosity curve due to the plasticising effect of PCM in the polymer matrix was observed. This downward shift was particularly pronounced at lower temperatures (140–95 °C). As a small molecule PCM can insert between polymer chains and reduce polymer-polymer interaction and enable increased movement of polymer strands. A previous study has shown a plasticising effect of 30% w/w PCM drug loading compared to neat Affinsol™ 15LV polymer. This was seen as changes to the mechanical properties of extruded filaments as well as a reduction in glass transition temperatures [7].

The extruded 30% w/w PCM-AFF sample followed a similar trend, although showing even lower complex viscosity values (Fig. 2). This was very likely due to the material exposed to mixing under shear and pressure in the Hot-Melt-Extruder (opposed to exposure to temperature only), resulting in increased mixing and distribution of PCM molecules in the polymer matrix, reducing polymer-polymer interactions.

Kolter reported a range of complex viscosity values of 8 10^2 to 10^4 Pa·s as suitable for extrusion on small scale extruders (Kolter et al., 2012). In order to meet this viscosity range, a process window of 190 – 155 °C would apply to the neat Affinisol™ 15LV polymer. This viscosity range was observed for the 30PCM-AFF PM from 190° to 135°C and the 30PCM-AFF extrudate from 190° to 125°C.

As macromolecules, the properties of polymers lie between that of elastic solids and viscous fluids [56]. When stress is applied to polymers, the resulting strain in the macromolecular network is time dependant. The resulting stress can be separated into the individual contributions of elastic and viscous behaviour of the polymer matrix. The Elastic Modulus represents the energy that is stored in material when stress is applied and also referred to as Storage modulus (G′). The energy that is lost via dissipation is referred to as the Viscous or Loss modulus (G”). For HME and 3D-printing applications, it is desirable when the polymer system is amenable to flow i.e., the viscous properties of a polymer dominate. When the elastic properties of the system dominate, HME can be problematic and e.g., die swell can occur. At the G′/G” crossover point (G′ = G”), the contribution of viscous and elastic properties are equal. At high temperatures (190 °C) all polymer systems showed behaviour dominated by viscous contributions (Fig. 3). The difference between viscous and elastic contribution for neat Affinisol™ 15LV across the entire temperature range was very small, seen in a low tendency to flow (even when the Loss Modulus dominated at temperatures > 160 °C, (Table 3). In contrast, both the PM 30PCM-AFF and the EX 30PCM-AFF sample showed a larger difference for viscous and elastic contributions, seen as a system that is more likely to flow when G” dominated compared to the neat polymer (Table 3).

3.2. Oscillatory frequency sweep

Oscillatory frequency sweeps of EX 30PCM-AFF samples showed a shear thinning behaviour (140 – 190 °C, Fig. 4A). At low temperatures and increasing angular frequency, the Elastic Modulus increased and dominated, whereas at high temperatures, the Viscous Modulus dominated until the angular frequency exceeded ~5 rad/s (Fig. 4B).

Process conditions for the HME-3D-printing process were selected in order to maintain a rheological behaviour with dominating viscous modulus within the ideal complex viscosity range reported by Kolter [57]. In order to keep shear stresses in the extruder low, a screw speed of 50 rpm was chosen.

Two process temperatures, 165 °C and 145 °C, were selected. The higher process temperature of 165 °C, was chosen, since the associated complex viscosity lay within the ideal complex viscosity range and it was above the G′/G” crossover temperature. Although the frequency sweep data indicated a wider range of dominating viscous behaviour at temperatures > 165 °C (Fig. 4), polymer discolouration and degradation at these temperatures has previously been reported [7]. The reported discolouration from amber to charred-black appearance of the polymer may adversely affect patient compliance when targeting OSD manufacture, but also affect drug release. However, the previous study only performed a visual assessment of the extruded polymer and further studies are required to characterise polymer degradation and associated

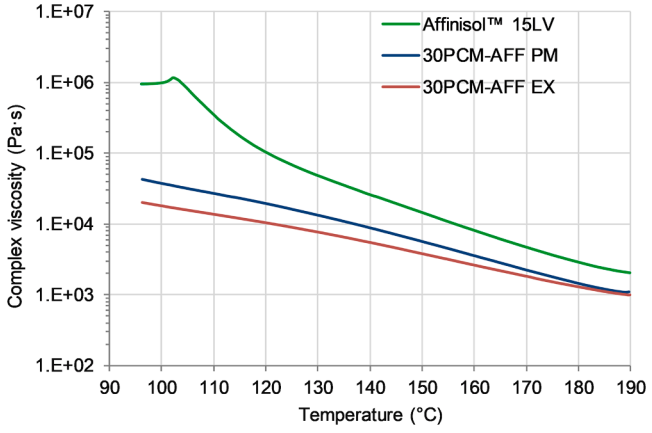

Fig. 2. Oscillatory temperature sweep from 190 °C to 95 °C: Complex viscosity versus Temperature (from high to low). Affinisol™ 15LV (green), PM 30PCM-AFF (blue) and EX 30PCM-AFF (red).

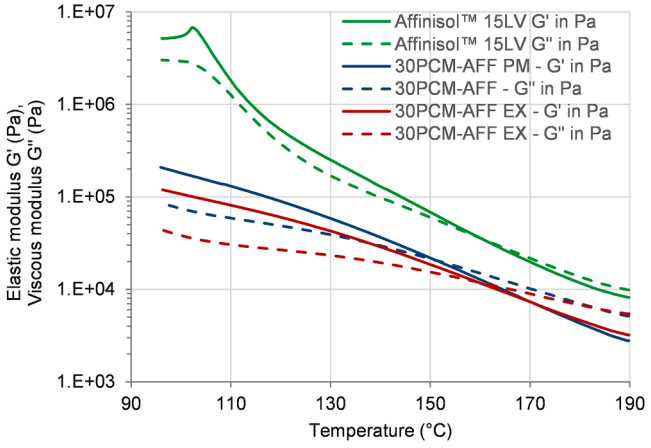

Fig. 3. Oscillatory temperature sweep – Elastic (G′, solid lines) and Viscous (G”, dashed lines) modulus versus temperature. Affinisol™ 15LV (green), physical mixture (PM, blue) and extrudate (EX, red) samples of 30PCM-AFF.

Table 3
Oscillatory temperature sweep – G_c crossover for Affinisol™ 15LV, physical mixture (PM) and extrudate (EX) samples of 30PCM-AFF.

Material	G_c Temp (°C) G_c = crossover	G_c (Pa)	Complex viscosity at G_c (Pa·s)
Affinisol™ 15LV	160.3	$3.5 \cdot 10^4$	8264
PM 30PCM-AFF	149.2	$2.6 \cdot 10^4$	5845
EX 30PCM-AFF	159.5	$1.2 \cdot 10^4$	2801

effects in detail.

The lower processing temperature of 145 °C was selected in order to reduce polymer discolouration and to assess contrasting rheological behaviour, with dominating Elastic Modulus.

3.3. HME-3DP

3.3.1. Initial printing trials

Initial printing studies were performed at 165 °C where the impact of slicer settings, such as layer height and print speed, on print quality was assessed. A simple tablet structure, a cylinder 13 mm by 4 mm, with a 50% Infill was printed (Fig. 5). Printing with a layer height of 0.2 mm, resulted in inconsistent material deposition, seen as a strong disruption of the infill pattern and a rough tablet surface (Fig. 5 A). In contrast, printing with a layer height of 0.4 mm resulted in good material deposition with highly controlled spatial resolution of the infill pattern (Fig. 5B).

The uniformity of mass and dimension of tablets was good with relative standard deviation (RSD) values below 1.6% (Table 4). However, over time, discolouration of the material was observed.

3.3.1.1. Process data. HME process data, torque and die pressure, were recorded during initial printing trials. The HME torque values recorded whilst processing at 165 °C were very consistent, ranging from 14% to 17% (Fig. 6). The associated die pressure when filling the metering device, ranged between 24 and 29 bar.

Batch reconciliation for the initial printing batch was performed by monitoring the weight of the LIW feeder, weighing the produced tablets and waste material from purging the filament free 3D printer and HME. Batch reconciliation showed that approximately 10 g of material were required for start-up of the process (Table S 2).

Table 4
Uniformity of mass for Cylinder 13 mm x 4 mm (50% Infill) printed with 30PCM-AFF at 165 °C (n = 10). Average, standard deviation (stdev), relative standard deviation (%RSD), minimum (MIN) and maximum (MAX) tablet weights, diameters and heights.

	Tablet weight (mg)	diameter (mm)	height (mm)
average	388.04	12.60	3.87
stdev	6.16	0.11	0.07
%RSD	**1.59**	**0.91**	**1.94**
MIN	379.30	12.46	3.77
MAX	397.70	12.84	3.97

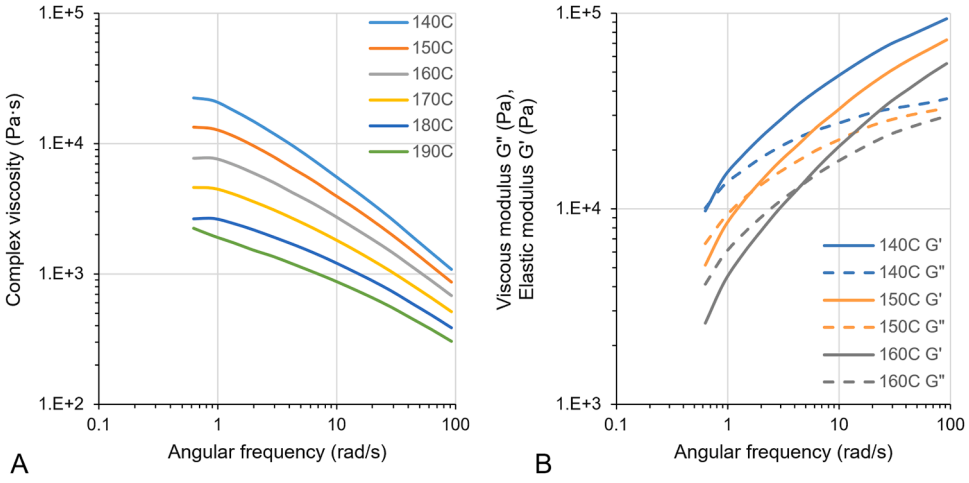

Fig. 4. Oscillatory frequency sweep of EX 30PCM-AFF at 140 (blue), 150 (orange), 160 (grey), 170 (yellow), 180 (dark blue) and 190 °C (green): A) Complex viscosity (Pa·s), B) Viscous (G") and Elastic (G′) modulus versus angular frequency (rad/s).

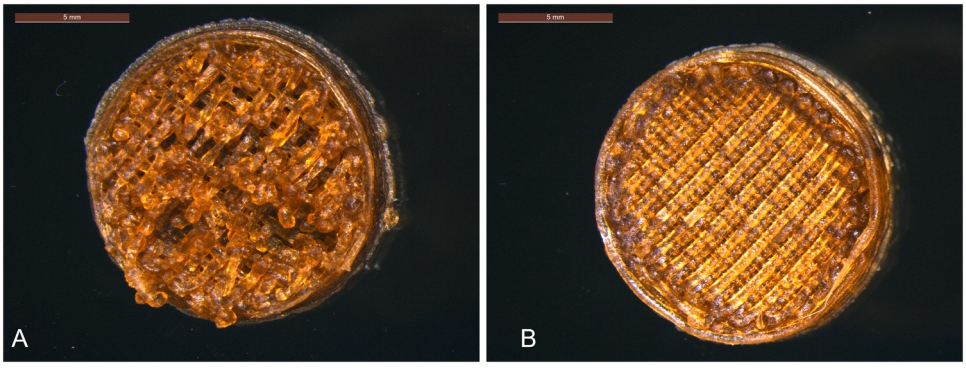

Fig. 5. 30PCM-AFF tablet structure A printed with a layer height of A) 0.2 mm and B) 0.4 mm at 20 mm/s and 165 °C and an infill percentage of 50%. Scale bar 5 mm.

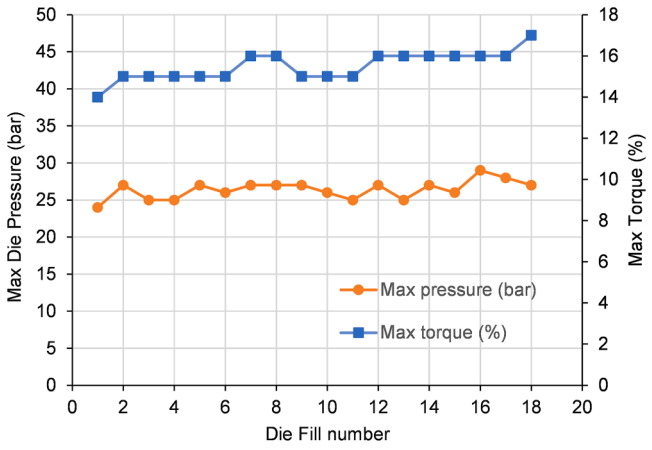

Fig. 6. HME process data from initial printing trials at 165 °C. Maximum torque (%, blue, square) and Maximum die pressure (bar, orange, circle) versus number of die fills.

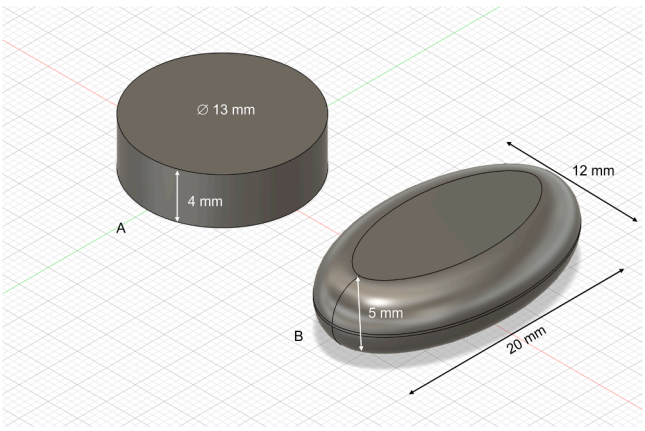

Fig. 7. 3D-printed tablet shapes: A) Cylinder, 13 mm × 4 mm; B) elliptical tablet shape, 20 mm × 12 mm x 5 mm, with rounded edges.

3.3.2. Printing at 145 °C, complex tablet shape

In an effort to minimize discolouration, process temperature was reduced, guided by previous work on this API-polymer system [58], to the minimum possible temperature of 145 °C. A more intricate, pharmaceutically relevant tablet shape (elliptical shape, 20 mm * 12 mm * 5 mm, rounded edges) was designed and printed. The size and volume of this tablet design was aimed to be in the region of a size 0 hard gelatine capsule.

3.3.2.1. Operating space – slicer settings at 145 °C. The limitation in terms of slicer settings on print quality of elliptically shaped tablets were investigated. Layer height settings ranged from 0.6 mm to 0.2 mm with associated linear print speeds of 20 mm/s and 40 mm/s.

Printing with a speed of 20 mm/s resulted in better quality infill than 40 mm/s, which was very likely due to the higher shear rate in the system at 40 mm/s. When assessing shear thinning behaviour of this formulation, strong shear thinning behaviour was observed at 140 °C with low complex viscosity values and high elastic modulus contributions (Fig. 4). In addition, the faster print speed is associated with shorter cooling times and therefore lower complex viscosity when the material is deposited. Slower cooling can also affect the tenacity, or stickiness, of the material, with material sticking excessively to adjacent deposited beads, resulting in disrupted material deposition and spatial resolution.

Poor quality infill was observed for a small layer height of ≤ 0.2 mm (Fig. 8A). The deposited bead of material was too thin and the associated complex viscosity too low to support its own weight. The associated high contribution of elastic modulus under these print conditions may have also disrupted layer formation in the printed object. Tablets completely lacked the infill pattern and presented with distorted elliptical dimensions. Layer height 0.6–0.4 mm resulted in good quality infill. In this case, the combination of material throughput, shear rate and cooling time were ideal for controlled deposition of the material, seen in high spatial resolution of the infill pattern. Layer height of 0.3 mm was better than 0.2 mm, but not as good as layer height of 0.4 mm. However, if a tablet was printed with a complete shell, the quality would still be acceptable. Particularly if subsequent processing steps may be added to product manufacture, such as a coating step. The fastest print was performed with a layer height of 0.6 mm and a print speed of 40 mm/s, taking 1 min 31 s to produce a tablet core weight of 418.2 mg (50% Infill).

3.3.2.2. Infill percentage versus tablet weight. Tablet structure B (Fig. 7) was printed with a layer height of 0.4 mm and 20 mm/s print speed at 145 °C. Tablet structures were printed without top or bottom layer in order to assess the quality of the infill. The relationship between tablet core weight and slicer Infill percentage settings was assessed by printing tablets with Infill percentage settings ranging from 20% to 70%. The average weight, standard deviation and relative standard deviation (% RSD) are reported in Table S 1, with % RSD values ≤ 5% (n = 3). Linear regression analysis showed a good fit for the linear relationship between tablet core weight and Infill percentage with an $r^2 = 0.9983$ (Fig. 10). The dose forms produced, typically have an amber to light brown appearance. This coloration was due to the Affinisol™ 15LV as previously shown [7].

3.3.2.3. HME process data – Printing at 145 °C. The HME process parameter values recorded whilst processing at 145 °C were not as consistent as when processed at the higher temperature of 165 °C. Torque values ranged from 22% to 32% and die pressure values when filling the metering device, ranged between 22 and 32 bar, with two outliers at 43 and 46 bar at the start of the process (Fig. 11). The rheological characterisation of the material at 145 °C showed dominating elastic modulus behaviour (Fig. 3) and also high sensitivity to shear (Fig. 4) compared to higher process temperatures (such as 165 °C), which may explain the high pressure variations observed during the process. In addition, the flow of polymer melt material in the metering device undergoes directional changes during processing very likely exacerbating the adverse (undesirable) rheological behaviour (at 145 °C) that very likely contributed to pressure fluctuations.

Batch reconciliation was performed on two days of printing at 145 °C. The equipment remained assembled for day 2 printing, therefore less material (8.6 g) was required for start-up of the equipment.

4. Discussion

The objective of this study was to demonstrate/investigate how a novel, filament free 3D printing system opens up the pharmaceutical formulation space and also simplifies the manufacturing process through a single manufacturing step reducing time and resource.

Manufacturing 3D printed tablets by means of the novel, filament-free 3D printer presented in this study, combines the two-step process of filament extrusion by HME and successive 3D printing process into a single step. The filament free 3D printer is composed of a small-scale extruder, equipped with a metering device to enable controlled layer by layer deposition of material onto a mobile print bed. The process development for this filament free 3D printer required consideration of the HME process parameters, but also of 3D printing process parameters, where due to the smaller nozzle sizes much higher shear rates are obtained. Standard practice for identifying a suitable HME process temperature is to work 20–40 °C above the glass transition temperature (Tg)

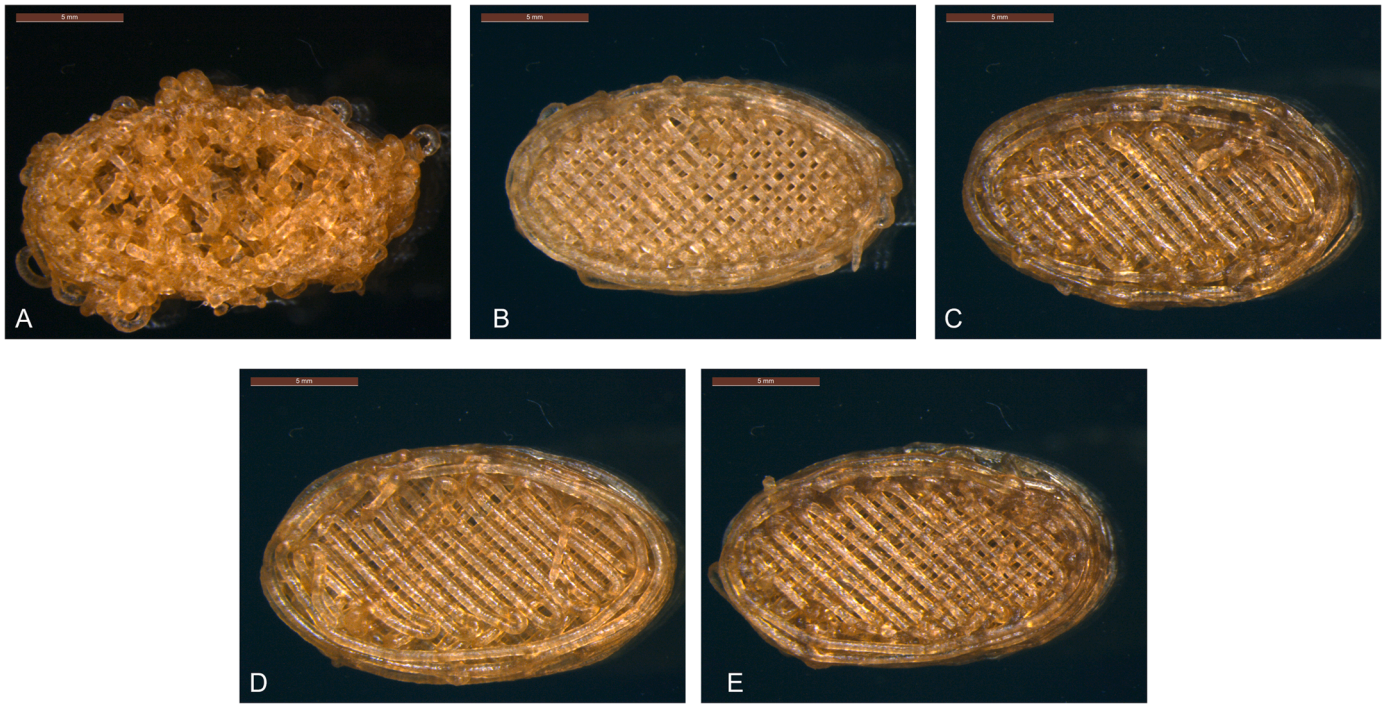

Fig. 8. Tablets 3D printed with 30PCM-AFF at 145 °C (0.4 mm nozzle): Layer height A) 0.2 mm, B) 0.3 mm, C) 0.4 mm, D) 0.5 mm, E) 0.6 mm. Scale bar 5 mm.

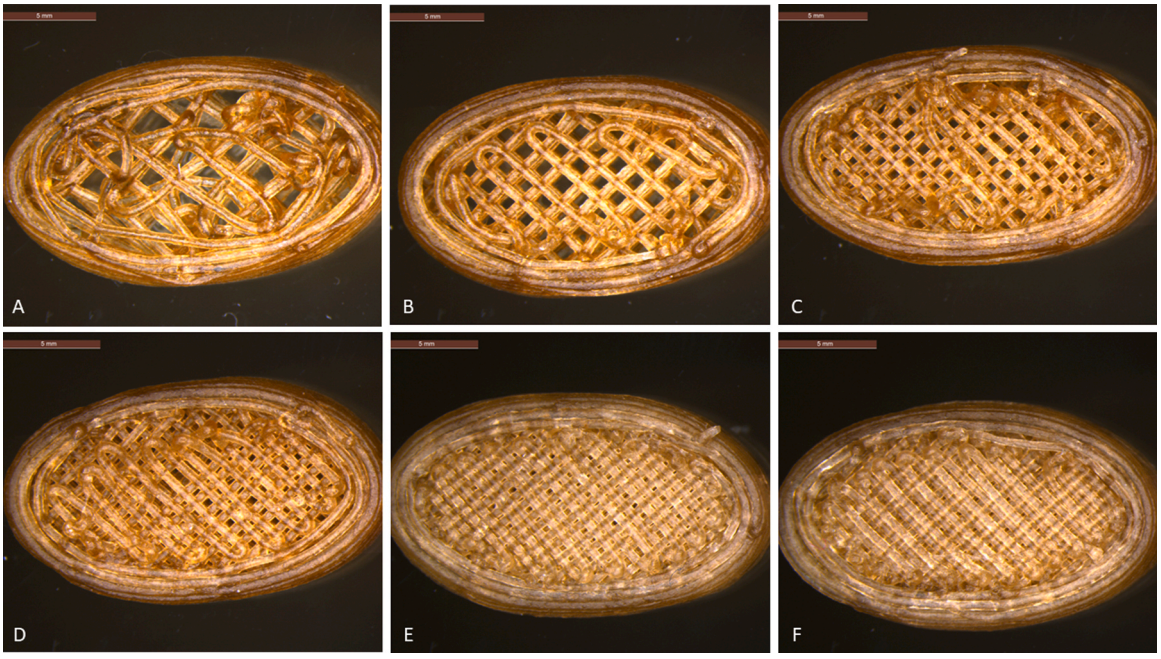

Fig. 9. Tablet shape B printed with 30PCM-AFF at 145 °C with different Infill percentage: A) 20%, B) 30%, C) 40%, D) 50%, E) 60% and F) 70% Infill. No top or bottom layers were printed. Scale bar 5 mm.

of the polymer [30,59]. This approach requires investigation of a large temperature range and lacks information on the viscoelastic properties of materials: the tendency of material to flow at temperature and under shear. Here, a rheological assessment of the formulation was performed instead. A broad temperature range exhibited ideal complex viscosity values ($8 * 10^2$ to 10^4 Pa·s, Fig. 2) for processing a 30PCM-AFF formulation on a small scale extruder [57,60].

Ideal viscoelastic properties of polymers during the 3D printing step differ from HME. For 3D printing, the material requires low enough viscosity to be extruded through a nozzle where the material is exposed to high shear rates [60], but as the material exits the nozzle and the shear is removed, good shape stability is required to prevent dripping or oozing [60–62]. After material deposition, the material must also be able to adhere to the print substrate in a manner that allows the release of the printed object, once the process is complete. The material must also be able to interdiffuse across the interface of adjacent layers to facilitate good layer to layer adhesion and mechanical stability [63]. This process involves flow and polymer chain diffusion and occurs in a time-dependant manner [21,64].

Than et al. [60], reported shear thinning behaviour of polymeric

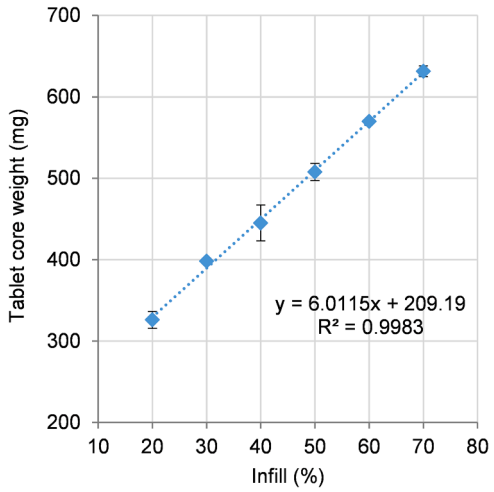

Fig. 10. Tablet core weight versus Infill percentage for 30PCM-AFF printed at 145 °C (n = 3).

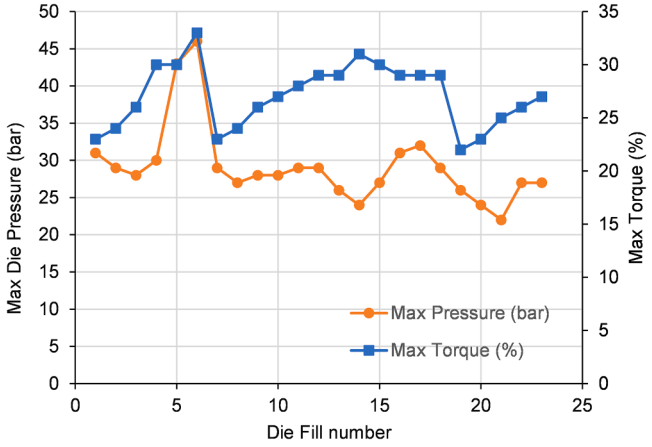

Fig. 11. HME process data from initial printing at 145 °C. Maximum torque (%, blue, square) and Maximum die pressure (bar, orange, circle) versus number of die fills.

systems suitable for FFF ranging from 295 to 31445 Pa·s (at 0.1 rad/s) or 13–1099 (at 100 rad/s). These findings were in line with previous studies by Isreb, Ilyes and Coogan suggesting that polymeric systems with a complex viscosity > 8000 Pa·s [65], > 1200 Pa·s [14] at 100 rad/s facilitated successful FFF printing. Elbadawi et al. [66] developed a rheological model, defining the in situ complex viscosity for printable formulations in the region of 10^2 Pa·s, which was also in agreement with in-line viscosity measurements by Coogan et al. [67]. The 30PCM-AFF formulation in this study also exhibited shear thinning behaviour (Fig. 4) in line with these findings. The shear thinning effect was more pronounced at 140 °C (with a change from 2.1 * 10^4 Pa·s at 0.1 rad/s to 1.1 * 10^3 Pa·s at 100 rad/s) compared to 160 °C (with a change from 7.7 * 10^3 Pa·s at 0.1 rad/s to 6.8 * 10^2 Pa·s at 100 rad/s).

However, it is not only the complex viscosity that impacts the printability or extrudability of polymeric systems. The viscoelastic properties, as in the elastic modulus (G′) and the viscous modulus (G″), impact the success of 3D printing processes. Calafel et al. proposed that the viscous modulus (G″) should dominate over the elastic modulus (G′) for successful printing of polymeric systems [64]: dominant elastic behaviour (G′ > G″) caused by a crystalline network caused clogging in the nozzle of an FFF printer. Assessing the viscoelastic properties of 30PCM-AFF across a wide temperature range (Fig. 3), identified 165 °C as the lowest temperature where the viscous modulus of the material dominated, material being amenable to flow and therefore desirable for extrusion [56,64]. When the formulation was tested at different frequencies, non-Newtonian, shear thinning behaviour was observed (Fig. 4). This behaviour was beneficial for shape stability when the material exits the nozzle during 3D printing: as the shear from the nozzle is removed, the viscosity increases preventing oozing and dripping from the nozzle [61]. Materials exhibiting high shear thinning also have a lower tendency to back-flow in the nozzle [27,28,60]. This was reflected in initial printing trials where simple, cylinder shaped tablets were printed (Fig. 7A) with very good uniformity of mass and dimensions (Table 4). Associated HME process data was indicative of a stable process, with only small variations in torque and die pressure values over the duration of tablet manufacture at 165 °C (Fig. 6). Printing at 165 °C failed at high print speeds of 40 mm/s and at layer heights of 0.2 mm (Fig. 5). Failure at the faster print speed was most likely due to the increased shear rate in the print nozzle during extrusion, resulting in a complex viscosity lacking sufficient structure to support deposited layers of material on the print bed.

In contrast, 3D printing of 30PCM-AFF via filament feedstock in a conventional FFF printer failed [7], despite low complex viscosity values (305 Pa·s) and high contributions of viscous modulus (Fig. 3) associated with the higher process temperature of 190 °C. Printing via filament feedstock may have been possible at lower print speeds, since reducing the print speed has shown to reduce the pressure drop in the hot end of an FFF printer [12]. However, this would increase the thermal load of the material potentially leading to drug and / or polymer degradation. The filament free 3D printer in this study was capable of printing this problematic formulation at significantly lower temperatures in a single manufacturing step.

A reduction in process temperature below 165 °C was sought due to the observed discolouration of the polymer during initial extrusion experiments. The lowest extrusion temperature of 30PCM-AFF mixture on a small scale extruder had previously been reported as 115 °C [58]. This low extrusion temperature was most likely possible due to the high screw speed of 200 rpm and the associated shear thinning behaviour of the formulation (Fig. 4), resulting in a reduced complex viscosity suitable for a small-scale extruder. In addition, since Affinisol™ 15LV has previously been reported as shear sensitive to degradation [7], this study aimed to keep the screw speed low. As a consequence, further printing studies were performed at 145 °C, a compromise to prevent discolouration but also reduce the overall contribution of the elastic modulus during extrusion and 3D printing.

The reduction in process temperature to 145 °C did not affect the quality of prints. In fact, a more complex, more pharmaceutically relevant, elliptical tablet shape with rounded edges was printed successfully and an excellent relationship of Infill percentage to tablet core weight was established (Fig. 10). The operating space for “layer height” in the Slicer Software was also identified and limits established (Fig. 8).

Despite the good quality and reliable printing performance at 145 °C (Fig. 10), the associated process data (torque and die pressure) showed large variations (Fig. 11), indicative of an unstable process. Backfilling of the HME channel, with material exiting the vent port were also observed at lower temperatures. This was most likely due to the viscoelastic behaviour of the polymer matrix. At 145 °C, the elastic modulus dominated the overall behaviour of the polymer system (Fig. 3, Fig. 4). A dominating elastic modulus has been reported to potentially cause problems during HME processes [30,56] but also during extrusion through an FFF printer nozzle [64]. However, this did not affect filling of the metering device (and potential impact on the uniformity of mass of printed tablets).

Conventional FFF printers operate with standardised filament diameters of 1.75 mm (or 2.85 mm) with linear print speeds ranging from 3 to up to 90 mm/s [7,8,12,39,47]. The maximum linear print speed cannot exceed 90 mm/s since printers cannot accelerate to higher speed for small objects, such as an OSD [68]. Although the linear print speed is most commonly reported in 3D printing studies, it is the volumetric flow

rate of the material during the printing process which gives a better representation of the material throughput in the printer. The volumetric flow rate relates to linear print speed and the area of the filament diameter in the printer. The maximum linear print speed for the 30PCM-AFF formulation resulting in good quality material deposition was a linear print speed of 20 mm/s (Section 3.6.1 and 3.6.2), equivalent to a volumetric flow rate of 370 mm^3/s (with a nozzle size of 0.4 mm and a layer height of 0.3 mm). Material deposition of the filament free 3D printer is faster than the corresponding volumetric flow rate of 216 mm^3/s of a conventional FFF printer (with a filament diameter of 1.75 mm at a linear speed of 90 mm/s) Table 5.

The filament free 3D printer presented in this study also offers a fully customisable HME mixing profile (with an integrated 3D printing step). This type of system offers the possibility to work with a wider range of formulation approaches. Tablet cores of ~400 mg were printed in times ranging from 90 s with a layer height of 0.6 mm to 5 mins with a layer height of 0.2 mm. The uniformity of mass was good with an RSD $\leq$ 5%, in line with pharmacopeial limits, despite a process that had not been fully optimized. The filament free printer also operates in continuous mode, allowing for flexible batch sizes. Batch reconciliation was good for both processing temperatures (Table S 2), with only 10 g of material required for start-up of the process. However, this could be reduced with shortening of the barrel length of the extruder.

The advantages of filament free 3D printing are, as described above, abundant. This case study demonstrates how a non-printable, ductile feedstock filament formulation was processed on a novel, filament-free 3D printer in a single manufacturing step. In the traditional two step manufacturing process (of filament and subsequent printing of the 3D object), the 3D printing step requires significantly higher process temperatures than the filament extrusion step, since the solid filament requires softening or melting via heat transfer in the hot end in a time dependant manner [2,21]. A single manufacturing step at reduced process temperature, reduces the temperature load of the material during the manufacturing process.

This study, relates material properties to HME-3D printing process parameters and print quality for a novel filament free 3D printer, identifying a valid process space for processing a 30PCM-AFF formulation.

5. Conclusion

The application of rheology screening to the HME 3D printing process development for a novel, filament free 3D printer, facilitated detection of appropriate processing conditions needing less material.

Single step 3D printing process of a 30PCM-AFF formulation, with unsuitable properties for processing via filament fabrication and FFF printing, generating pharmaceutically acceptable oral dose forms was demonstrated. The operating space for HME process parameters and slicer settings for successfully processing the formulation on the novel printer were established.

This study illustrates how a filament free 3D printer opens up the pharmaceutical formulation space, facilitating a single, streamlined melt extrusion process with reduced thermal load of the material.

This work forms part of the broader aim of the EPSRC Future Manufacturing Research HUB at CMAC. The project aims to implement integrated continuous, laboratory scale manufacturing platforms by the means of crystal engineering of a model drug, coupled with polymer processing steps to deliver enhanced physical properties for biopharmaceutics performance. It forms the basis for future work within the HUB, how coupling crystal engineering with polymer processing may facilitate future performance-based design and continuous manufacture of structured particulate products [29].

CRediT authorship contribution statement

Elke Prasad: Writing – review & editing, Writing – original draft, Visualization, Methodology, Investigation, Formal analysis, Data curation, Conceptualization. **John Robertson:** Writing – review & editing. **Alastair J. Florence:** Funding acquisition. **Gavin W. Halbert:** Writing – review & editing, Supervision.

Table 5
Comparison of linear print speeds and volumetric flow rate of a conventional FFF printer and the filament free 3D printer.

	Volumetric flow rate (mm^3/s)			
Linear print speed	10 mm/s	20 mm/s	40 mm/s	90 mm/s
FFF printer	24	48	96	217
filament free 3D printer	185	370	739	1663

Declaration of Competing Interest

The authors declare the following financial interests/personal relationships which may be considered as potential competing interests: John Robertson reports equipment, drugs, or supplies was provided by The Dow Chemical Company. Gavin Halbert, John Robertson has patent #Intellectual Property Office UK, patent application number 2101534.2 pending to University of Strathclyde.

Data Availability

All data underpinning this publication are openly available from the University of Strathclyde KnowledgeBase at https://doi.org/10.15129/bdce0b29–70f1–46a0-bf27-f3562a4f5f9e.

Acknowledgements

The authors would like to acknowledge that this work was carried out in the CMAC National Facility supported by the EPSRC [Grant ref EP/P006965/1] and by UKRPIF (UK Research Partnership Fund) award from the Higher Education Funding Council for England (HEFCE) [Grant ref HH13054]. G. W. Halbert is funded by Cancer Research UK [C149/A20496]. Further funding support for this project was obtained from the Scottish Enterprise High Growth Spinout Programme Covid Response fund [reference PS6215C012]. We would like to thank Dow Chemicals for the donation of Affinisol™ 15LV polymer. We would like to thank Ali Anwar for his work on the filament free 3D printer and Natasha Thomson for supporting the rheology work.

Appendix A. Supporting information

Supplementary data associated with this article can be found in the online version at doi:10.1016/j.addma.2023.103803.

References

[1] A. Samaro, B. Shaqour, N.M. Goudarzi, M. Ghijs, L. Cardon, M.N. Boone, B. Verleije, K. Beyers, V. Vanhoorne, P. Cos, C. Vervaet, Can filaments, pellets and powder be used as feedstock to produce highly drug-loaded ethylene-vinyl acetate 3D printed tablets using extrusion-based additive manufacturing? Int. J. Pharm. 607 (2021), 120922 https://doi.org/10.1016/j.ijpharm.2021.120922.

[2] N. Dumpa, A. Butreddy, H. Wang, N. Komanduri, S. Bandari, M.A. Repka, 3D printing in personalized drug delivery: an overview of hot-melt extrusion-based fused deposition modeling, Int. J. Pharm. 600 (2021), 120501, https://doi.org/10.1016/j.ijpharm.2021.120501.

[3] C. Parulski, O. Jennotte, A. Lechanteur, B. Evrard, Challenges of fused deposition modeling 3D printing in pharmaceutical applications: where are we now? Adv. Drug Deliv. Rev. 175 (2021), 113810 https://doi.org/10.1016/j.addr.2021.05.020.

[4] G.G. Pereira, S. Figueiredo, A.I. Fernandes, J.F. Pinto, Polymer selection for hot-melt extrusion coupled to fused deposition modelling in, Pharmaceutics, Pharmaceutics 12 (9) (2020) 795, https://doi.org/10.3390/pharmaceutics12090795.

[5] E. Prasad, J. Robertson, G.W. Halbert, Solid dispersions: improving drug performance through tablet micro-structure design, American Association of Pharmaceutical Scientists (AAPS) 2021 PharmSci 360, Hybrid event: Virtual and

Philadelphia, United States, 2021, ⟨https://pureportal.strath.ac.uk/en/publications/solid-dispersions-improving-drug-performance-through-tablet-micro⟩.
[6] M. Sadia, B. Arafat, W. Ahmed, R.T. Forbes, M.A. Alhnan, Channelled tablets: an innovative approach to accelerating drug release from 3D printed tablets, J. Control Release 269 (2018) 355–363, https://doi.org/10.1016/j.jconrel.2017.11.022.
[7] E. Prasad, M.T. Islam, D.J. Goodwin, A.J. Megarry, G.W. Halbert, A.J. Florence, J. Robertson, Development of a hot-melt extrusion (HME) process to produce drug loaded Affinisol™ 15LV filaments for fused filament fabrication (FFF) 3D printing, Addit. Manuf. 29 (2019), 100776, https://doi.org/10.1016/j.addma.2019.06.027.
[8] K. Pietrzak, A. Isreb, M.A. Alhnan, A flexible-dose dispenser for immediate and extended release 3D printed tablets, Eur. J. Pharm. Biopharm. 96 (2015) 380–387, https://doi.org/10.1016/j.ejpb.2015.07.027.
[9] A. Goyanes, J. Wang, A. Buanz, R. Martinez-Pacheco, R. Telford, S. Gaisford, A. W. Basit, 3D printing of medicines: engineering novel oral devices with unique design and drug release characteristics, Mol. Pharm. 12 (11) (2015) 4077–4084, https://doi.org/10.1021/acs.molpharmaceut.5b00510.
[10] A. Goyanes, F. Fina, A. Martorana, D. Sedough, S. Gaisford, A.W. Basit, Development of modified release 3D printed tablets (printlets) with pharmaceutical excipients using additive manufacturing, Int J. Pharm. 527((1–2) (2017) 21–30, https://doi.org/10.1016/j.ijpharm.2017.05.021.
[11] C.I. Gioumouxouzis, A. Baklavaridis, O.L. Katsamenis, C.K. Markopoulou, N. Bouropoulos, D. Tzetzis, D.G. Fatouros, A 3D printed bilayer oral solid dosage form combining metformin for prolonged and glimepiride for immediate drug delivery, Eur. J. Pharm. Sci. 120 (2018) 40–52, https://doi.org/10.1016/j.ejps.2018.04.020.
[12] S. Henry, A. Samaro, F.H. Marchesini, B. Shaqour, J. Macedo, V. Vanhoorne, C. Vervaet, Extrusion-based 3D printing of oral solid dosage forms: Material requirements and equipment dependencies, Int. J. Pharm. 598 (2021), 120361, https://doi.org/10.1016/j.ijpharm.2021.120361.
[13] J.M. Nasereddin, N. Wellner, M. Alhijjaj, P. Belton, S. Qi, Development of a simple mechanical screening method for predicting the feedability of a pharmaceutical FDM 3D printing filament, Pharm. Res. 35 (8) (2018) 151, https://doi.org/10.1007/s11095-018-2432-3.
[14] K. Ilyes, N.K. Kovacs, A. Balogh, E. Borbas, B. Farkas, T. Casian, G. Marosi, I. Tomuta, Z.K. Nagy, The applicability of pharmaceutical polymeric blends for the fused deposition modelling (FDM) 3D technique: Material considerations-printability-process modulation, with consecutive effects on in vitro release, stability and degradation, Eur. J. Pharm. Sci. 129 (2019) 110–123, https://doi.org/10.1016/j.ejps.2018.12.019.
[15] G. Verstraete, A. Samaro, W. Grymonpre, V. Vanhoorne, B. Van Snick, M.N. Boone, T. Hellemans, L. Van Hoorebeke, J.P. Remon, C. Vervaet, 3D printing of high drug loaded dosage forms using thermoplastic polyurethanes, Int J. Pharm. 536 (1) (2018) 318–325, https://doi.org/10.1016/j.ijpharm.2017.12.002.
[16] A. Samaro, P. Janssens, V. Vanhoorne, J. Van Renterghem, M. Eeckhout, L. Cardon, T. De Beer, C. Vervaet, Screening of pharmaceutical polymers for extrusion-Based Additive Manufacturing of patient-tailored tablets, Int. J. Pharm. 586 (2020), 119591, https://doi.org/10.1016/j.ijpharm.2020.119591.
[17] J. Macedo, A. Samaro, V. Vanhoorne, C. Vervaet, J.F. Pinto, Processability of poly (vinyl alcohol) based filaments with paracetamol prepared by hot-melt extrusion for additive manufacturing, J. Pharm. Sci. 109 (12) (2020) 3636–3644, https://doi.org/10.1016/j.xphs.2020.09.016.
[18] J. Aho, J.P. Botker, N. Genina, M. Edinger, L. Arnfast, J. Rantanen, Roadmap to 3D-printed oral pharmaceutical dosage forms: feedstock filament properties and characterization for fused deposition modeling, J. Pharm. Sci. 108 (1) (2019) 26–35, https://doi.org/10.1016/j.xphs.2018.11.012.
[19] N. Gottschalk, M. Bogdahn, M. Harms, J. Quodbach, Brittle polymers in Fused Deposition Modeling: an improved feeding approach to enable the printing of highly drug loaded filament, Int. J. Pharm. 597 (2021), 120216, https://doi.org/10.1016/j.ijpharm.2021.120216.
[20] M.A. Azad, D. Olawuni, G. Kimbell, A.Z.M. Badruddoza, M.S. Hossain, T. Sultana, Polymers for extrusion-based 3D printing of pharmaceuticals: a holistic materials-process perspective, Pharmaceutics 12 (2) (2020), https://doi.org/10.3390/pharmaceutics12020124.
[21] G.M. Khalid, N. Billa, Solid dispersion formulations by FDM 3D printing-a review, Pharmaceutics 14 (4) (2022), https://doi.org/10.3390/pharmaceutics14040690.
[22] M. Spoerk, F. Arbeiter, I. Raguž, C. Holzer, J. Gonzalez-Gutierrez, Mechanical Recyclability of Polypropylene Composites Produced by Material Extrusion-Based Additive Manufacturing, 11(8) (2019) 1318, https://www.mdpi.com/2073–4360/11/8/1318.
[23] L.J. Tan, W. Zhu, K. Zhou, Recent progress on polymer materials for additive manufacturing 30 (43) (2020) 2003062, https://doi.org/10.1002/adfm.202003062.
[24] C. Korte, J. Quodbach, Formulation development and process analysis of drug-loaded filaments manufactured via hot-melt extrusion for 3D-printing of medicines, Pharm. Dev. Technol. 23 (10) (2018) 1117–1127, https://doi.org/10.1080/10837450.2018.1433208.
[25] J. Quodbach, M. Bogdahn, J. Breitkreutz, R. Chamberlain, K. Eggenreich, A.G. Elia, N. Gottschalk, G. Gunkel-Grabole, L. Hoffmann, D. Kapote, T. Kipping, S. Klinken, F. Loose, T. Marquetant, H. Windolf, S. Geißler, T. Spitz, Quality of FDM 3D printed medicines for pediatrics: considerations for formulation development, filament extrusion, printing process and printer design, Ther. Innov. Regul. Sci. 56 (6) (2022) 910–928, https://doi.org/10.1007/s43441-021-00354-0.
[26] E. Prasad, J. Robertson, G.W. Halbert, Printability of pharmaceutical polymers in FDM 3D printers, Virtual PharmSci: APS international conference, Virtual, 2021,
[27] E.M. Mackay, The importance of rheological behavior in the additive manufacturing technique material extrusion, J. Rheol. 62 (2018) 1549–1561, https://doi.org/10.1122/1.5037687.
[28] E.L. Gilmer, D. Miller, C.A. Chatham, C. Zawaski, J.J. Fallon, A. Pekkanen, T. E. Long, C.B. Williams, M.J. Bortner, Model analysis of feedstock behavior in fused filament fabrication: enabling rapid materials screening, Polymer 152 (2018) 51–61, https://doi.org/10.1016/j.polymer.2017.11.068.
[29] E. Prasad, J. Robertson, G.W. Halbert, Improving consistency for a mefenamic acid immediate release formulation, J. Pharm. Sci. 109 (11) (2020) 3462–3470, https://doi.org/10.1016/j.xphs.2020.08.012.
[30] E. Prasad, J. Robertson, G.W. Halbert, Mefenamic acid solid dispersions: impact of formulation composition on processing parameters, product properties and performance, Int J. Pharm. 616 (2022), 121505, https://doi.org/10.1016/j.ijpharm.2022.121505.
[31] S. Palekar, P.K. Nukala, S.M. Mishra, T. Kipping, K. Patel, Application of 3D printing technology and quality by design approach for development of age-appropriate pediatric formulation of baclofen, Int J. Pharm. 556 (2019) 106–116, https://doi.org/10.1016/j.ijpharm.2018.11.062.
[32] C. Wei, N.G. Solanki, J.M. Vasoya, A.V. Shah, A.T.M. Serajuddin, Development of 3D printed tablets by fused deposition modeling using polyvinyl alcohol as polymeric matrix for rapid drug release, J. Pharm. Sci. 109 (4) (2020) 1558–1572, https://doi.org/10.1016/j.xphs.2020.01.015.
[33] A. Melocchi, F. Parietti, A. Maroni, A. Foppoli, A. Gazzaniga, L. Zema, Hot-melt extruded filaments based on pharmaceutical grade polymers for 3D printing by fused deposition modeling, Int J. Pharm. 509 (1–2) (2016) 255–263, https://doi.org/10.1016/j.ijpharm.2016.05.036.
[34] A. Maroni, A. Melocchi, F. Parietti, A. Foppoli, L. Zema, A. Gazzaniga, 3D printed multi-compartment capsular devices for two-pulse oral drug delivery, J. Control Release 268 (2017) 10–18, https://doi.org/10.1016/j.jconrel.2017.10.008.
[35] M. Fanous, S. Gold, S. Muller, S. Hirsch, J. Ogorka, G. Imanidis, Simplification of fused deposition modeling 3D-printing paradigm: Feasibility of 1-step direct powder printing for immediate release dosage form production, Int. J. Pharm. 578 (2020), 119124, https://doi.org/10.1016/j.ijpharm.2020.119124.
[36] J. Wu, N. Chen, F. Bai, Q. Wang, Preparation of poly (vinyl alcohol)/poly (lactic acid)/hydroxyapatite bioactive nanocomposites for fused deposition modeling, Polym. Compos. 39 (2018) E508–E518.
[37] N. Venkataraman, S. Rangarajan, M.J. Matthewson, B. Harper, A. Safari, S. C. Danforth, G. Wu, N. Langrana, S. Guceri, A. Yardimci, Feedstock material property – process relationships in fused deposition of ceramics (FDC), Rapid Prototyp. J. 6 (4) (2000) 244–253, https://doi.org/10.1108/13552540010373344.
[38] R.C.R. Beck, P.S. Chaves, A. Goyanes, B. Vukosavljevic, A. Buanz, M. Windbergs, A. W. Basit, S. Gaisford, 3D printed tablets loaded with polymeric nanocapsules: an innovative approach to produce customized drug delivery systems, Int J. Pharm. 528 (1–2) (2017) 268–279, https://doi.org/10.1016/j.ijpharm.2017.05.074.
[39] T.C. Okwuosa, D. Stefaniak, B. Arafat, A. Isreb, K.W. Wan, M.A. Alhnan, A lower temperature FDM 3D printing for the manufacture of patient-specific immediate release tablets, Pharm. Res 33 (11) (2016) 2704–2712, https://doi.org/10.1007/s11095-016-1995-0.
[40] T.C. Okwuosa, B.C. Pereira, B. Arafat, M. Cieszynska, A. Isreb, M.A. Alhnan, Fabricating a shell-core delayed release tablet using dual FDM 3D printing for patient-centred therapy, Pharm. Res 34 (2) (2017) 427–437, https://doi.org/10.1007/s11095-016-2073-3.
[41] A. Goyanes, A. Fernandez-Ferreiro, A. Majeed, N. Gomez-Lado, A. Awad, A. Luaces-Rodriguez, S. Gaisford, P. Aguiar, A.W. Basit, PET/CT imaging of 3D printed devices in the gastrointestinal tract of rodents, Int J. Pharm. 536 (1) (2018) 158–164, https://doi.org/10.1016/j.ijpharm.2017.11.055.
[42] J. Zhang, X. Feng, H. Patil, R.V. Tiwari, M.A. Repka, Coupling 3D printing with hot-melt extrusion to produce controlled-release tablets, Int J. Pharm. 519 (1–2) (2017) 186–197, https://doi.org/10.1016/j.ijpharm.2016.12.049.
[43] Y. Yang, H. Wang, H. Li, Z. Ou, G. Yang, 3D printed tablets with internal scaffold structure using ethyl cellulose to achieve sustained ibuprofen release, Eur. J. Pharm. Sci. 115 (2018) 11–18, https://doi.org/10.1016/j.ejps.2018.01.005.
[44] M. Bertolino, D. Battegazzore, R. Arrigo, A. Frache, Designing 3D printable polypropylene: material and process optimisation through rheology, Addit. Manuf. 40 (2021), 101944, https://doi.org/10.1016/j.addma.2021.101944.
[45] G.G. Pereira, S. Figueiredo, A.I. Fernandes, J.F. Pinto, Polymer selection for hot-melt extrusion coupled to fused deposition modelling in pharmaceutics, Pharmaceutics (2020), https://doi.org/10.3390/pharmaceutics12090795.
[46] M. Sadia, A. Sośnicka, B. Arafat, A. Isreb, W. Ahmed, A. Kelarakis, M.A. Alhnan, Adaptation of pharmaceutical excipients to FDM 3D printing for the fabrication of patient-tailored immediate release tablets, Int. J. Pharm. 513 (1) (2016) 659–668, https://doi.org/10.1016/j.ijpharm.2016.09.050.
[47] B. Arafat, M. Wojsz, A. Isreb, R.T. Forbes, M. Isreb, W. Ahmed, T. Arafat, M. A. Alhnan, Tablet fragmentation without a disintegrant: a novel design approach for accelerating disintegration and drug release from 3D printed cellulosic tablets, Eur. J. Pharm. Sci. 118 (2018) 191–199, https://doi.org/10.1016/j.ejps.2018.03.019.
[48] E. Prasad, J. Robertson, G.W. Halbert, Quality control test for pharmaceutical feedstock material for FDM 3D printers, Virtual PharmSci: APS international conference, Virtual, 2021, ⟨https://pureportal.strath.ac.uk/en/publications/quality-control-test-for-pharmaceutical-feedstock-material-for-fd⟩.
[49] T. Xie, L.S. Taylor, Effect of temperature and moisture on the physical stability of binary and ternary amorphous solid dispersions of celecoxib, J. Pharm. Sci. 106 (1) (2017) 100–110, https://doi.org/10.1016/j.xphs.2016.06.017.

[50] C. Cardona, A.H. Curdes, A.J. Isaacs, Effects of filament diameter tolerances in fused filament fabrication, IU J. Undergrad. Res. 2 (1) (2016) 44–47, https://doi.org/10.14434/iujur.v2i1.20917.
[51] S. Bandari, D. Nyavanandi, N. Dumpa, M.A. Repka, Coupling hot melt extrusion and fused deposition modeling: critical properties for successful performance, Adv. Drug Deliv. Rev. 172 (2021) 52–63, https://doi.org/10.1016/j.addr.2021.02.006.
[52] FabRx, M3DIMAKER™. ⟨https://www.fabrx.co.uk/technologies/⟩. (Accessed 20FEB2023 2023).
[53] A. Goyanes, N. Allahham, S.J. Trenfield, E. Stoyanov, S. Gaisford, A.W. Basit, Direct powder extrusion 3D printing: fabrication of drug products using a novel single-step process, Int. J. Pharm. 567 (2019), 118471, https://doi.org/10.1016/j.ijpharm.2019.118471.
[54] M. Pistone, G.F. Racaniello, I. Arduino, V. Laquintana, A. Lopalco, A. Cutrignelli, R. Rizzi, M. Franco, A. Lopedota, N. Denora, Direct cyclodextrin-based powder extrusion 3D printing for one-step production of the BCS class II model drug niclosamide, Drug Deliv. Transl. Res. 12 (8) (2022) 1895–1910, https://doi.org/10.1007/s13346-022-01124-7.
[55] Y. Zheng, F. Deng, B. Wang, Y. Wu, Q. Luo, X. Zuo, X. Liu, L. Cao, M. Li, H. Lu, S. Cheng, X. Li, Melt extrusion deposition (MED™) 3D printing technology - a paradigm shift in design and development of modified release drug products, Int J. Pharm. 602 (2021), 120639, https://doi.org/10.1016/j.ijpharm.2021.120639.
[56] J. Aho, J.P. Boetker, S. Baldursdottir, J. Rantanen, Rheology as a tool for evaluation of melt processability of innovative dosage forms, Int J. Pharm. 494 (2) (2015) 623–642, https://doi.org/10.1016/j.ijpharm.2015.02.009.
[57] K. Kolter, M. Karl, A. Gryczke, Hot-Melt Extrusion with BASF Pharma Polymers, 2nd Revised and Enlarged Edition ed., BASF The Chemical Company, Ludwigshafen, Germany, 2012,
[58] E. Bordos, M.T. Islam, A.J. Florence, G.W. Halbert, J. Robertson, Use of terahertz-raman spectroscopy to determine solubility of the crystalline active pharmaceutical ingredient in polymeric matrices during hot melt extrusion, Mol. Pharm. 16 (10) (2019) 4361–4371, https://doi.org/10.1021/acs.molpharmaceut.9b00703.
[59] C. Kulkarni, A. Kelly, T. Gough, V. Jadhav, K. Singh, A. Paradkar, Application of hot melt extrusion for improving bioavailability of artemisinin a thermolabile drug, Drug Dev. Ind. Pharm. 44 (2017) 1–9, https://doi.org/10.1080/03639045.2017.1386200.
[60] Y.M. Than, S. Suriyarak, V. Titapiwatanakun, Rheological investigation of hydroxypropyl cellulose–based filaments for material extrusion 3D printing, Polymers (2022), https://doi.org/10.3390/polym14061108.
[61] R. Arrigo, A. Frache, FDM printability of PLA based-materials: the key role of the rheological behavior, Polymeers 14 (9) (2022), https://doi.org/10.3390/polym14091754.
[62] A. Zidan, A. Alayoubi, S. Asfari, J. Coburn, B. Ghammraoui, S. Aqueel, C.N. Cruz, M. Ashraf, Development of mechanistic models to identify critical formulation and process variables of pastes for 3D printing of modified release tablets, Int J. Pharm. 555 (2019) 109–123, https://doi.org/10.1016/j.ijpharm.2018.11.044.
[63] R. Arrigo, M. Bartoli, G. Malucelli, Poly(lactic acid)–biochar biocomposites: effect of processing and filler content on rheological, Therm., Mech. Prop. 12 (4) (2020) 892. ⟨https://www.mdpi.com/2073-4360/12/4/892⟩.
[64] I. Calafel, R.H. Aguirresarobe, M.I. Peñas, A. Santamaria, M. Tierno, J.I. Conde, B. Pascual, Searching for rheological conditions for FFF 3D printing with PVC based flexible compounds, Materials 13 (1) (2020), https://doi.org/10.3390/ma13010178.
[65] A. Isreb, K. Baj, M. Wojsz, M. Isreb, M. Peak, M.A. Alhnan, 3D printed oral theophylline doses with innovative 'radiator-like' design: impact of polyethylene oxide (PEO) molecular weight, Int. J. Pharm. 564 (2019) 98–105, https://doi.org/10.1016/j.ijpharm.2019.04.017.
[66] M. Elbadawi, T. Gustaffson, S. Gaisford, A.W. Basit, 3D printing tablets: predicting printability and drug dissolution from rheological data, Int. J. Pharm. 590 (2020), 119868, https://doi.org/10.1016/j.ijpharm.2020.119868.
[67] T. Coogan, D. Kazmer, In-line rheological monitoring of fused deposition modeling, J. Rheol. 63 (2019) 141–155, https://doi.org/10.1122/1.5054648.
[68] T. Feuerbach, S. Kock, M. Thommes, Characterisation of fused deposition modeling 3D printers for pharmaceutical and medical applications, Pharm. Dev. Technol. 23 (10) (2018) 1136–1145, https://doi.org/10.1080/10837450.2018.1492618.